

BEVDISTILL: CROSS-MODAL BEV DISTILLATION FOR MULTI-VIEW 3D OBJECT DETECTION

Zehui Chen¹, Zhenyu Li², Shiquan Zhang³, Liangji Fang³, Qinhong Jiang³, Feng Zhao^{1*}

¹ University of Science and Technology of China

² Harbin Institute of Technology

³ SenseTime Research

lovesnow@mail.ustc.edu.cn, fzhaao956@ustc.edu.cn

zhenyuli17@hit.edu.cn

{zhangshiquan, fangliangji, jiangqinhong}@senseauto.com

ABSTRACT

3D object detection from multiple image views is a fundamental and challenging task for visual scene understanding. Owing to its low cost and high efficiency, multi-view 3D object detection has demonstrated promising application prospects. However, accurately detecting objects through perspective views is extremely difficult due to the lack of depth information. Current approaches tend to adopt heavy backbones for image encoders, making them inapplicable for real-world deployment. Different from the images, LiDAR points are superior in providing spatial cues, resulting in highly precise localization. In this paper, we explore the incorporation of LiDAR-based detectors for multi-view 3D object detection. Instead of directly training a depth prediction network, we unify the image and LiDAR features in the Bird-Eye-View (BEV) space and adaptively transfer knowledge across non-homogenous representations in a teacher-student paradigm. To this end, we propose **BEVDistill**, a cross-modal BEV knowledge distillation (KD) framework for multi-view 3D object detection. Extensive experiments demonstrate that the proposed method outperforms current KD approaches on a highly-competitive baseline, BEVFormer, without introducing any extra cost in the inference phase. Notably, our best model achieves 59.4 NDS on the nuScenes test leaderboard, achieving new state-of-the-arts in comparison with various image-based detectors.

Code will be available at <https://github.com/zehuichen123/BEVDistill>.

1 INTRODUCTION

3D object detection, aiming at localizing objects in the 3D space, is a crucial ingredient for 3D scene understanding. It has been widely adopted in various applications, such as autonomous driving (Chen et al., 2022a; Shi et al., 2020; Wang et al., 2021b), robotic navigation (Antonello et al., 2017), and virtual reality (Schuemie et al., 2001). Recently, multi-view 3D object detection has drawn great attention thanks to its low cost and high efficiency. As images offer a discriminative appearance and rich texture with dense pixels, detectors can easily discover and categorize the objects, even in a far distance. Despite the promising deployment advantage, accurately localizing instances from camera view only is extremely difficult, mainly due to the ill-posed nature of monocular imagery. Therefore, recent approaches adopt heavy backbones (*e.g.*, ResNet-101-DCN (He et al., 2016), VoVNetV2 (Lee & Park, 2020)) for image feature extraction, making it inapplicable for real-world applications.

LiDAR points, which capture precise 3D spatial information, provide natural guidance for camera-based object detection. In light of this, recent works (Guo et al., 2021b; Peng et al., 2022) start to explore the incorporation of point clouds in 3D object detection for performance improvement. One line of work (Wang et al., 2019b) projects each points to the image to form depth map labels, and subsequently trains a depth estimator to explicitly extract the spatial information. Such a paradigm generates intermediate products, *i.e.*, depth prediction maps, therefore introducing extra computational cost. Another line of work (Chong et al., 2021) is to leverage the teacher-student paradigm for

*Corresponding author

knowledge transfer. (Chong et al., 2021) projects the LiDAR points to the image plane, constructing a 2D input for the teacher model. Since the student and teacher models are exactly structurally identical, feature mimicking can be naturally conducted under the framework. Although it solves the alignment issue across different modalities, it misses the opportunity of pursuing a strong LiDAR-based teacher, which is indeed important in the knowledge distillation (KD) paradigm. Recently, UVTR (Li et al., 2022a) propose to distill the cross-modal knowledge in the voxel space, while maintaining the structure of respective detectors. However, it directly forces the 2D branch to imitate the 3D features, ignoring the divergence between different modalities.

In this work, by carefully examining the non-homogenous features represented in the 2D and 3D spaces, we explore the incorporation of knowledge distillation for multi-view 3D object detection. Yet, there are two technical challenges. First, the views of images and LiDAR points are different, *i.e.*, camera features are in the perspective view, while LiDAR features are in the 3D/bird’s-eye view. Such a view discrepancy indicates that a natural one-to-one imitation (Romero et al., 2014) may not be suitable. Second, RGB images and point clouds hold respective representations in their own modalities. Therefore, it can be suboptimal to mimic features directly, which is commonly adopted in the 2D detection paradigm (Yang et al., 2022a; Zhang & Ma, 2020).

We address the above challenges by designing a cross-modal BEV knowledge distillation framework, namely **BEVDistill**. Instead of constructing a separate depth estimation network or explicitly projecting one view into the other one, we convert all features to the BEV space, maintaining both geometric structure and semantic information. Through the shared BEV representation, features from different modalities are naturally aligned without much information loss. After that, we adaptively transfer the spatial knowledge through both *dense* and *sparse* supervision: (i) we introduce soft foreground-guided distillation for non-homogenous dense feature imitation, and (ii) a sparse style instance-wise distillation paradigm is proposed to selectively supervise the student by maximizing the mutual information.

Experimental results on the competitive nuScenes dataset demonstrate the superiority and generalization of our BEVDistill. For instance, we achieve 3.4 NDS and 2.7 NDS improvements on a competitive multi-view 3D detector, BEVFormer (Li et al., 2022c), under the single-frame and multi-frame settings, respectively. Besides, we also present extensive experiments on lightweight backbones, as well as detailed ablation studies to validate the effectiveness of our method. Notably, our best model reaches 59.4 NDS on nuScenes test leaderboard, achieving new state-of-the-art results among all the published multi-view 3D detectors.

2 RELATED WORK

2.1 VISION-BASED 3D OBJECT DETECTION

Vision-based 3D object detection aims to detect object locations, scales, and rotations, which is of great importance in autonomous driving (Xie et al., 2022; Jiang et al., 2022; Zhang et al., 2022) and augmented reality (Azuma, 1997). One line of work is to detect 3D boxes directly from single images. Mono3D (Chen et al., 2016) utilizes traditional methods to lift 2D objects into 3D space with semantic and geometrical information. In the consideration that objects located at different distances appear on various scales, D4LCN (Ding et al., 2020) proposes to leverage depth prediction for convolutional kernel learning. Recently, FCOS3D (Wang et al., 2021a) extends the classical 2D paradigm FCOS (Tian et al., 2019b) into monocular 3D object detection. It transforms the regression targets into the image domain by predicting its 2D-based attributes. Further, PGD (Wang et al., 2022b) introduces relational graphs to improve the depth estimation for object localization. MonoFlex (Zhang et al., 2021) argues that objects located at different positions should not be treated equally and presents auto-adjusted supervision.

Another line of work predicts objects from multi-view images. DETR3D (Wang et al., 2022c) first incorporates DETR (Carion et al., 2020) into 3D detection by introducing a novel concept: 3D reference points. After that, Graph-DETR3D (Chen et al., 2022b) extends it by enriching the feature representations with dynamic graph feature aggregation. Different from the above methods, BEVDet (Huang et al., 2021) leverages the Lift-splat-shoot (Phlion & Fidler, 2020) to explicitly project images into the BEV space, followed by a traditional 3D detection head. Inspired by the recently developed attention mechanism, BEVFormer (Li et al., 2022c) automates the cam2bev process with

a learnable attention manner and achieves superior performance. PolarFormer (Jiang et al., 2022) introduces polar coordinates into the model construction of BEV space and greatly improves the performance. Moreover, BEVDepth (Li et al., 2022b) improves BEVDet by explicitly supervising depth prediction with projected LiDAR points and achieves state-of-the-art performance.

2.2 KNOWLEDGE DISTILLATION IN OBJECT DETECTION

Most KD approaches for object detection focus on transferring knowledge among two homogenous detectors by forcing students’ predictions to match those of the teacher (Chen et al., 2017; Dai et al., 2021; Zheng et al., 2022). More recent works (Guo et al., 2021a; Wang et al., 2019a) find that imitation of feature representations is more effective for detection. A vital challenge is to determine which feature regions should be distilled from the teacher model. FGGI (Wang et al., 2019a) chooses features that are covered by anchor boxes whose IoU with GT is larger than a certain threshold. PGD (Yang et al., 2022a) only focuses on a few key predictive regions using a combination of classification and regression scores as a measure of quality.

Despite a large number of works discussing the KD in object detection, only a few of them consider the multi-modal setting. MonoDistill (Chong et al., 2021) projects the points into the image plane and applies a modified image-based 3D detector as the teacher to distill knowledge. Such a paradigm solves the alignment issue naturally, however, it misses the chance to pursue a much stronger point-based teacher model. LIGA-stereo (Guo et al., 2021b) leverages the information of LiDAR by supervising the BEV representation of the vision-based model with the intermediate output from the SECOND (Yan et al., 2018). Recently, UVTR (Li et al., 2022a) presents a simple approach by directly regularizing the voxel representations between the student and teacher models. Both of them choose to mimic the feature representations across the models, while ignoring the divergence between different modalities.

3 METHODS

In this section, we introduce our proposed BEVDistill in detail. We first give an overview of the whole framework in Figure 1 and clarify the model designs of the teacher and student model in Section 3.1. After that, we present the cross-modal knowledge distillation approach in Section 3.2, which consists of two modules: dense feature distillation and sparse instance distillation.

3.1 BASELINE MODEL

Student Model. We adopt current state-of-the-art camera-based detector, BEVFormer (Li et al., 2022c), as our student model. It consists of an image backbone for feature extraction, a spatial cross-attention module for cam2bev view transformation, and a transformer head for 3D object detection. Besides, it provides a temporal cross-attention module to perceive subsequential multi-frame information for better predictions.

Teacher Model. In order to keep consistent with the student model, we select Object-DGCNN (Wang & Solomon, 2021) as our teacher model. For simplicity and generality, we replace the DGCNN attention with a vanilla multi-scale attention module. It first casts 3D points into the BEV plane and then conducts one-to-one supervision with transformer-based label assignment. We train the model by initializing it from a pre-trained CenterPoint model.

3.2 BEVDISTILL

BEVDistill follows the common knowledge distillation paradigm, with a 3D point cloud detector as teacher and an image detector as student. Different from previous knowledge distillation methods, which keep the same architecture for both student and teacher models (except for backbone), BEVDistill explores a more challenging setting with non-homogenous representations.

3.2.1 DENSE FEATURE DISTILLATION

In order to conduct dense supervision for feature distillation, we first need to determine the BEV features generated from both models. For the student, we directly adopt the BEV features maps

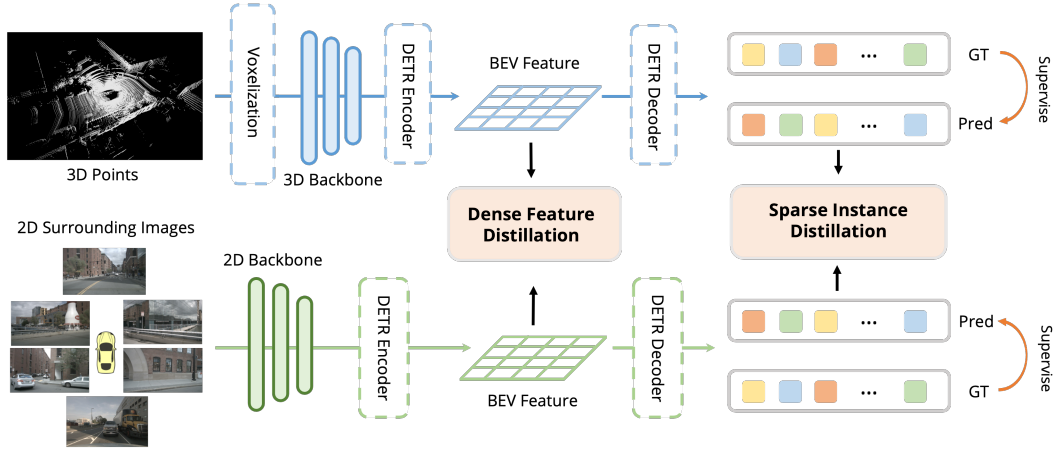


Figure 1: The overall architecture of the proposed BEVDistill consists of three main components: a transformer-based LiDAR detector, a transformer-based image detector, and the proposed cross-modal distillation modules. It follows the teacher-student paradigm with both RGB images and LiDAR points as the inputs and keeps the original structure of respective model structures.

F^{2D} produced by the BEVTransformerEncoder. In order to align the feature representations between the teacher and student, we choose the same BEV feature F^{3D} outputted by the transformer encoder for the teacher model. Different from LIGA-Stereo (Guo et al., 2021b) which directly mimics the BEV features extracted from the 3D backbone, we postpone such supervision after the transformer encoder (illustrated in Figure 1), which offers more opportunities for the network to align information across different modalities.

Previous works (Romero et al., 2014; Li et al., 2022a) directly force the student to mimic the feature map from the teacher and achieve significant performance improvement:

$$L_{feat} = \frac{1}{H \times W} \sum_i^H \sum_j^W \|F_{ij}^{3D} - F_{ij}^{2D}\|_2, \quad (1)$$

where H, W denotes the width and height of the distilled feature map, and $\|\cdot\|_2$ is the L_2 norm. However, such a strategy may not work well under the cross-modal feature setting. Although the view discrepancy is eliminated by projecting both features into the BEV plane, there is still domain discrepancy between different modalities: *despite the same scenes being captured with the point clouds and images with careful alignment, the representation itself can be diverse under different modalities.* For instance, images holds pixels for both foreground and backgrounds regions, however LiDAR points only appears when there exists objects to reflect the ray.

Consider that the regional 3D features can hold meaningful information only if the point exists, we regularize the distillation within the foreground regions. Besides, we notice that the boundary of foreground could also provides useful information. Therefore, instead of performing hard supervision on each foreground region, we introduce a soft-supervision manner similar to that in (Zhou et al., 2019). Concretely, we draw Gaussian distribution for each ground truth center (x_i, y_i) in the BEV space with,

$$w_{i,x,y} = \exp\left(-\frac{(x_i - \hat{x}_i)^2 + (y_i - \hat{y}_i)^2}{2\sigma_i^2}\right), \quad (2)$$

where σ_i is a constant (set to 2 by default), indicating the object size standard deviation. Since the feature maps are class-agnostic, we merge all $w_{i,x,y}$ into one single mask W . For overlapping regions among different $w_{i,x,y}$ at the same position, we simply take the maximum value of them.

After that, we enforce the student to mimic the feature with the foreground-guided mask W for dense feature distillation:

$$L_{feat} = \frac{1}{H \times W \times \sum max(W_{i,j})} \sum_i^H \sum_j^W max(W_{ij}) ||F_{ij}^{3D} - F_{ij}^{2D}||_2. \quad (3)$$

This foreground-guided re-weight strategy allows the model to focus on the foreground regions from the teacher, and at the same time avoid imitation of useless empty 3D features in the background regions. Such a manner is counter to the finding in previous homogeneous knowledge distillation works (Yang et al., 2022c).

3.2.2 SPARSE INSTANCE DISTILLATION

Instance-level distillation can be easily conducted under the dense prediction setting, where only a pixel-to-pixel mapping is needed for supervision. However, both the student and teacher models in BEVDistill act in a sparse-prediction style. Therefore, a set-to-set mapping is required to ensure instance-level distillation. To achieve the goal, we simply follow the practice in (Wang & Solomon, 2021) to construct the correspondence between the student and teacher predictions. Specifically, suppose the categorical and localization predictions output by the i^{th} query from the teacher model are c_i^T and b_i^T , and the student can be represented as c_i^S and b_i^S , a permutation of $\hat{\sigma}$ can be found between the output set of the teacher and the student with the lowest cost:

$$\hat{\sigma} = \arg \min \sum_i^N \mathcal{L}_{match}(y_i, \hat{y}_i), \quad (4)$$

where $\mathcal{L}_{match}(y_i, \hat{y}_i)$ is a pair-wise matching cost, which is defined as:

$$\mathcal{L}_{match}(y_i, \hat{y}_i) = -\log c_{\sigma(i)}^S(c_i^T) + ||b_i^T, b_{\sigma(i)}^S||_1. \quad (5)$$

However, we empirically find such a vanilla distillation approach works poorly in a cross-domain supervision manner. There are two main issues that impede the model from further performance improvement. On one hand, not all predictions from the teacher should be treated equally as valuable cues, since most of the predictions are false positives with a low classification score. On the other hand, though the classification logits can represent rich knowledge (Hinton et al., 2015), it may not hold when the input data are different. Directly distilling these prediction will introduce great noise to the model and deteriorate the performance. To tackle the problem, we exploit reliable quality score derived from the teacher model to measure the importance of the instance-level pseudo labels and use the score as soft re-weighted factors to eliminate the potential noise predictions made by the teacher. Specifically, we consider the classification score c_i (categorical information) and the IoU between the prediction b_i^{pred} and the ground truth b_i^{GT} (localization information) together to formulate the quality-score q_i :

$$q_i = (c_i)^\gamma \cdot \text{IoU}(b_i^{GT}, b_i^{pred})^{1-\gamma}. \quad (6)$$

The quality score serves as an indicator to guide the student on which teacher's predictions should be paid more weight. Therefore, the final instance-level distillation can be written as:

$$\mathcal{L}_{inst} = \sum_i^N -q_i (\alpha \mathcal{L}_{cls}(c_{\sigma(i)}^S, c_i^T) + \beta \mathcal{L}_{box}(b_i^T, b_{\sigma(i)}^S)), \quad (7)$$

where \mathcal{L}_{cls} is the KL divergence loss, \mathcal{L}_{box} is the L_1 loss in (Wang & Solomon, 2021), and α, β are reweighted factors to balance the supervision (set to 1.0 and 0.25 by default). Given that the prediction probability mass function over classes contains richer information than one-hot labels, student models are proven to be benefited from such extra supervision (Hinton et al., 2015). However, this low dimensional prediction distribution (number of classes) means that only a few amount of knowledge is encoded, thus limiting the knowledge that can be transferred, especially under the cross-modal setting. Besides, the representational knowledge is often structured, with implicit complex interdependencies across different dimensions, while the KL objective treats all dimensions

independently. To overcome the problem, instead of minimizing the KL divergence over two distributions, we choose to directly maximize the mutual information (MI) between the representations h^S, h^T at the penultimate layer (before logits) from the teacher and student networks:

$$I(h^S; h^T) = \text{KL}(p(h^T, h^S) || \mu(h^T)v(h^S)), \quad (8)$$

where $p(h^T, h^S)$ is the joint distribution and the marginal distributions $\mu(h^T), v(h^S)$. We then define a distribution q conditioned on η that captures whether the pair is congruent ($q(\eta = 1)$) or incongruent ($q(\eta = 0)$):

$$q(h^T, h^S | \eta = 1) = p(h^T, h^S), q(h^T, h^S | \eta = 0) = \mu(h^T)v(h^S). \quad (9)$$

With Bayes' rule, we can obtain the posterior for $\eta = 1$:

$$q(\eta = 1 | h^T, h^S) = \frac{p(h^T, h^S)}{p(h^T, h^S) + \mu(h^T)v(h^S)}, \quad (10)$$

By taking the logarithm of both sides, we have

$$\log q(\eta = 1 | h^T, h^S) \leq \log \frac{p(h^T, h^S)}{p(h^T, h^S) + \mu(h^T)v(h^S)} = I(h^T, h^S). \quad (11)$$

Therefore, the objective can be transformed to maximize the lower bound of MI. Since there is no closed form for $q(\eta = 1 | h^T, h^S)$, we utilize a neural network g , called critic (Tian et al., 2019a) to approximate with NCE loss (see Appendix A for detailed implementation):

$$L_{cls}(h^T, h^S) = E_{q(h^T, h^S | \eta=1)}[\log g(h^T, h^S)] + E_{q(h^T, h^S | \eta=0)}[\log (1 - g(h^T, h^S))]. \quad (12)$$

To this end, the final sparse instance distillation loss can be represented as:

$$\mathcal{L}_{inst} = \sum_i^N -q_i (\alpha \mathcal{L}_{cls}(h_i^S, h_i^T) + \beta \mathcal{L}_{box}(b_i^T, b_{\sigma(i)}^S)). \quad (13)$$

4 EXPERIMENTS

4.1 DATASET AND EVALUATION METRICS

We conduct the experiments on the NuScenes dataset (Caesar et al., 2020), which is one of the most popular datasets for 3D object detection. It consists of 700 scenes for training, 150 scenes for validation, and 150 scenes for testing. For each scene, it includes 6 camera images (front, front left, front right, back left, back right, back) to cover the whole viewpoint, and a 360° LiDAR point cloud. Camera matrixes including both intrinsic and extrinsic are provided, which establish a one-to-one correspondence between each 3D point and the 2D image plane. There are 23 categories in total, and only 10 classes are utilized to compute the final metrics according to the official evaluation code.

We adopt the official evaluation toolbox provided by nuScenes. We report nuScenes Detection Score (NDS) and mean Average Precision (mAP), along with mean Average Translation Error (mATE), mean Average Scale Error (mASE), mean Average Orientation Error (mAOE), mean Average Velocity Error (mAVE), mean Average Attribute Error (mAAE) in our experiments. The NDS score is a weighted sum of mean Average Precision (mAP) and the aforementioned True Positive (TP) metrics, which is defined as $NDS = \frac{1}{10}[5 \times mAP + \sum_{mTP \in TP} (1 - \min(1, mTP))]$.

4.2 IMPLEMENTATION DETAILS

Our codebase is built on MMDetection3D (Contributors, 2020) toolkit. All models are trained on 8 NVIDIA A100 GPUs. We first train the 3D detector with a voxel size of $(0.1m, 0.1m, 0.2m)$ followed in (Yin et al., 2021). During the distillation phase, the batch size is set to 1 per GPU with an initial learning rate of 2e-4. Unless otherwise specified, we train the models for $2 \times$ schedule (24 epochs) with a cyclic policy. The input image size is set to 1600×900 and the grid size of the BEV plane in BEVFormer is set to 128×128 . FP16 training is enabled for GPU memory management.

Table 1: Comparison of recent distillation works on the nuScenes validation set with ResNet-50 image backbone. * indicates our own re-implementation with modifications.

Detector	Setting	NDS↑	mAP↑
BEVFormer	Teacher	67.4	61.5
	Student	42.3	35.2
	FitNet (Romero et al., 2014)	41.1	34.4
	Set2Set (Wang & Solomon, 2021)	41.0	33.1
	MonoDistill* (Chong et al., 2021)	42.9	36.4
	UVTR (Li et al., 2022a)	43.1	36.2
BEVFormer-T	BEVDistill (Ours)	45.7(+3.4)	38.6(+3.4)
	Teacher	67.4	61.5
	Student	48.8	38.3
	FitNet (Romero et al., 2014)	48.0	37.3
	Set2Set (Wang & Solomon, 2021)	47.9	37.5
	MonoDistill* (Chong et al., 2021)	49.5	39.0
	UVTR (Li et al., 2022a)	50.1	39.4
	BEVDistill (Ours)	51.5(+2.7)	40.7(+2.4)

4.3 MAIN RESULTS

We first implement BEVFormer and BEVFormer-T on the nuScenes validation subset with ResNet-50 backbone and compare BEVDistill with other knowledge distillation methods. The final results are shown in Table 1. Our BEVDistill greatly boosts its vanilla student model, BEVFormer, by more than 3.4/2.3 mAP and 3.4/2.7 NDS, respectively, without introducing any extra inference cost. Classical and effective distillation methods like FitNet ([Romero et al., 2014](#)), fail to bring any enhancement and even deteriorate the final performance, *i.e.*, -1.2% NDS. The Set2Set ([Wang & Solomon, 2021](#)) also gets struck in the detection accuracy (-1.3% NDS) due to the miss consideration of the divergence between different modality features. UVTR ([Li et al., 2022a](#)), which is the first work to leverage 3D points for multi-view 3D object detection, manages to get an 0.8 NDS improvement. However, it only focuses on feature-based distillation while missing the potential benefits in other aspects. We also reimplement MonoDistill ([Chong et al., 2021](#)) by extending its monocular version to a multi-view one, yielding an improvement of 0.7 NDS.

4.4 COMPARISON WITH STATE-OF-THE-ARTS

In addition to offline results, we also report the detection performance on nuScenes test leaderboard compared to various multi-view 3D detection approaches to further explore the potential of BEVDistill. The results are shown in Table 2. Our final model is based on current state-of-the-art model BEVDepth with an input image size of 640×1600 . We adopt ConvNeXt-base ([Liu et al., 2022d](#)) as our image encoder with a BEV space of 256×256 . The model is trained 20 epochs with CBGS and no test-time augmentation is applied. It surpasses all other detectors, including the recently developed PETRv2, BEVFormer, and BEVDet4D by more than 1.0 NDS, achieving new state-of-the-art on this competitive benchmark.

4.5 ABLATION STUDIES

In this section, we provide detailed ablation studies on different components of our model. For efficiency, we adopt BEVFormer-R50 as base model with $1\times$ schedule on 1/2 training subset.

4.5.1 MAIN ABLATIONS

To understand how each module contributed to the final detection performance in BEVDistill, we test each component independently and report its performance in Table 3. The overall baseline starts from 42.2 NDS. When dense feature distillation is applied, the NDS is raised by 2.5 points, which

Table 2: Comparison of recent works on the nuScenes testing set. “L” and “C” indicate LiDAR and Camera, respectively. \ddagger denotes our reimplementation borrowed from BEVDet.

Method	M.	NDS	mAP	mATE	mASE	mAOE	mAVE	mAAE	Reference
PointPillar	L	45.3	30.5	-	-	-	-	-	CVPR2019
CenterPoint	L	65.5	58.0	-	-	-	-	-	CVPR2021
BEVFusion	L+C	72.9	70.2	0.239	0.329	0.260	0.134	0.153	Arxiv2022c
FCOS3D	C	42.8	35.8	0.690	0.249	0.452	1.434	0.124	ICCVW2021a
Ego3RT	C	47.3	42.5	0.549	0.264	0.433	1.014	0.145	ECCV2022
DETR3D	C	47.9	41.2	0.641	0.255	0.394	0.845	0.133	CoRL2022c
BEVDet	C	48.8	42.4	0.524	0.242	0.373	0.950	0.148	Arxiv2021
G-DETR3D	C	49.5	42.5	0.621	0.251	0.386	0.790	0.128	MM2022b
PETR	C	50.4	44.1	0.593	0.249	0.384	0.808	0.132	ECCV2022a
UVTR	C	55.1	47.2	0.577	0.253	0.391	0.508	0.123	NeurIPS2022a
BEVDet4D	C	56.9	45.1	0.511	0.241	0.386	0.301	0.121	Arxiv2022
BEVFormer	C	56.9	48.1	0.582	0.256	0.375	0.378	0.126	ECCV2022c
PETRv2	C	58.2	49.0	0.561	0.243	0.361	0.343	0.120	Arxiv2022b
BEVDepth \ddagger	C	58.9	49.1	0.484	0.245	0.377	0.320	0.132	Arxiv2022b
+ BEVDistill	C	59.4	49.8	0.472	0.247	0.378	0.326	0.125	-

Table 3: Effectiveness of each component in BEVDistill. Results are reported on BEVFormer-R50 with standard $2 \times$ schedule setting.

	Dense Feature Distill	Sparse Instance Distill	NDS \uparrow	mAP \uparrow	mAOE \downarrow
a			42.3	35.2	0.428
b	✓		44.7	38.0	0.416
c		✓	43.9	37.1	0.410
d	✓	✓	45.7	38.6	0.399

validates the finding that disentangling the foreground regions with soft supervision can greatly promote the student’s detection ability. Then, we add the sparse instance distillation, which brings us a 1.7% NDS enhancement. Finally, the NDS score achieves 45.7 when all components are applied, yielding a 3.4 % absolute improvement, validating the effectiveness of BEVDistill.

4.5.2 ABLATIONS ON DENSE FEATURE DISTILLATION

Comparison with other feature-based distillation mechanisms.

Feature-based distillation methods have been extensively explored in both image classification (Hinton et al., 2015) and object detection tasks (Yang et al., 2022b;c). Therefore, we compare our dense feature distillation module with other competitive feature-based distillation approaches. The results are shown in Table 4. FitNet distills all pixels across 2D and 3D features with equal supervision, yielding little improvement. FGD (Yang et al., 2022b) is current state-of-the-art knowledge distillation approach in 2D object detection. However, it neglects the divergence between different modalities across features, therefore gets the worse performance. UVTR (Li et al., 2022a) also mimics the features directly but it only selects positive regions (query points) for feature imitation. Compared with the above methods, BEVDistill considers both modality divergence and region importance for feature imitation, providing the highest accuracy.

Strategies on foreground mask generation.

As mentioned in Section 3.2.1, not all positions in BEV feature representation should be treated equally. How to select the most informative regions for feature imitation is also non-trivial. Hence, we provide detailed experiments on how to generate the foreground imitation mask for distillation. Intuitively, we can directly select the center points of the ground truth objects (GT-Center) or the

Table 4: Comparison on feature-based knowledge distillation approaches.

Method	NDS	mAP	mAOE
-	37.5	33.3	0.515
FitNet	37.8	34.4	0.549
FGD	36.5	32.9	0.534
UVTR	38.1	34.5	0.513
BEVDistill	38.9	34.9	0.501

Table 5: Comparison on foreground mask generation approaches.

Method	NDS	mAP	mAOE
-	37.5	33.3	0.515
GT-Center	37.7	34.2	0.546
Query-Center	38.1	34.4	0.513
Pred-Heatmap	38.6	34.5	0.533
GT-Heatmap	38.9	34.9	0.501

query reference points (Query-Center) as imitation instances. However, such a strategy directly abandons most areas, which may contain useful information. Therefore, we attempt to convert such a ‘hard’ decision into the ‘soft’ manner with a heatmap mask, which can be the model classification prediction from the teacher (Pred-Heatmap) or the ground truth heatmap (GT-Heatmap). The final results are shown in Table 5. The soft foreground mask generation is much better compared to the hard one. We choose the GT-Heatmap strategy in our experiments due to its highest score.

4.5.3 ABLATIONS ON SPARSE INSTANCE DISTILLATION

Table 6: Ablations on loss selection for classification and regression branches.

cls	reg	NDS	mAP	mAOE
CE	-	35.8	31.7	0.544
-	L1	38.1	33.9	0.521
CE	L1	37.0	32.7	0.531
InfoNCE	L1	39.1	34.6	0.474

Table 7: Ablations on critic g selection and pair generation.

critic g	Pair	NDS	mAP
-	-	37.5	33.3
NCS Loss	Pos	38.0	33.7
CE Loss	Pos	35.8	31.7
InfoNCE Loss	Pos + Neg	38.6	34.5

Ablations on the instance distillation loss.

Instance-level distillation is a necessary module in detection-based knowledge distillation. However, such a component has been seldom discussed in a transformer-based sparse prediction setting. In this ablation, we conduct detailed experiments on the loss selection in Table 6. We first conduct the commonly adopted cross-entropy and L1 loss for the classification and regression branches. The result is surprisingly lower than its vanilla baseline. When adding them respectively, we figure out that the cross-entropy is the key issue leading to performance degradation. To avoid the problem, we replace it with the InfoNCE loss along with the contrastive paradigm, and an immediate improvement is observed, which validates our assumption in Section 3.2.2.

Strategies on selection of critic g .

Since most self-supervised learning approaches are based on homogenous representations, exploring the suitable contrastive paradigm for cross-modality is important. Note that features located in the same positions in the 2D and 3D BEV feature maps are considered positive pairs while the rest are negative pairs. We compare three prototypes of critic g and report the results in Table 7. We first adopt the classic InfoNCE loss, which provides the most improvement. We also conduct experiments on positive pairs only with NCS (negative cosine similarity) and CE (cross-entropy) loss, while gets little enhancement, validating the proof in Section 3.2.2.

5 CONCLUSION

In this paper, we introduce a cross-modal knowledge distillation framework for multi-view 3D object detection, namely BEVDistill. It unifies different modalities in the BEV space to ease the modal alignment and feature imitation. With the dense feature distillation module, it can effectively transfer rich teacher knowledge to the student across 2D and 3D data. BEVDistill also explores a sparse instance distillation approach under the transformer-based detection paradigm. Without bells and whistles, it achieves new state-of-the-art performance on the competitive nuScenes test leaderboard.

ACKNOWLEDGMENTS

This work was supported by the JKW Research Funds under Grant 20-163-14-LZ-001-004-01, and the Anhui Provincial Natural Science Foundation under Grant 2108085UD12. We acknowledge the support of GPU cluster built by MCC Lab of Information Science and Technology Institution, USTC.

REFERENCES

- Morris Antonello, Marco Carraro, Marco Pierobon, and Emanuele Menegatti. Fast and robust detection of fallen people from a mobile robot. In *IROS*, pp. 4159–4166, 2017.
- Ronald T Azuma. A survey of augmented reality. *Presence: teleoperators & virtual environments*, 6(4):355–385, 1997.
- Holger Caesar, Varun Bankiti, Alex H Lang, Sourabh Vora, Venice Erin Liang, Qiang Xu, Anush Krishnan, Yu Pan, Giancarlo Baldan, and Oscar Beijbom. nuScenes: A multimodal dataset for autonomous driving. In *CVPR*, pp. 11621–11631, 2020.
- Nicolas Carion, Francisco Massa, Gabriel Synnaeve, Nicolas Usunier, Alexander Kirillov, and Sergey Zagoruyko. End-to-end object detection with transformers. In *ECCV*, pp. 213–229, 2020.
- Guobin Chen, Wongun Choi, Xiang Yu, Tony Han, and Manmohan Chandraker. Learning efficient object detection models with knowledge distillation. In *NeurIPS*, volume 30, 2017.
- Xiaozhi Chen, Kaustav Kundu, Ziyu Zhang, Huimin Ma, Sanja Fidler, and Raquel Urtasun. Monocular 3D object detection for autonomous driving. In *CVPR*, pp. 2147–2156, 2016.
- Zehui Chen, Zhenyu Li, Shiquan Zhang, Liangji Fang, Qinghong Jiang, Feng Zhao, Bolei Zhou, and Hang Zhao. AutoAlign: Pixel-instance feature aggregation for multi-modal 3D object detection. In *IJCAI*, 2022a.
- Zehui Chen, Zhenyu Li, Shiquan Zhang, Liangji Fang, Qinghong Jiang, and Feng Zhao. Graph-DETR3D: Rethinking overlapping regions for multi-view 3D object detection. In *ACM MM*, pp. 5999–6008, 2022b.
- Zhiyu Chong, Xinzhu Ma, Hong Zhang, Yuxin Yue, Haojie Li, Zhihui Wang, and Wanli Ouyang. MonoDistill: Learning spatial features for monocular 3D object detection. In *ICLR*, 2021.
- MMDetection3D Contributors. MMDetection3D: OpenMMLab next-generation platform for general 3D object detection. <https://github.com/open-mmlab/mmdetection3d>, 2020.
- Xing Dai, Zeren Jiang, Zhao Wu, Yiping Bao, Zhicheng Wang, Si Liu, and Erjin Zhou. General instance distillation for object detection. In *CVPR*, pp. 7842–7851, 2021.
- Mingyu Ding, Yuqi Huo, Hongwei Yi, Zhe Wang, Jianping Shi, Zhiwu Lu, and Ping Luo. Learning depth-guided convolutions for monocular 3D object detection. In *CVPR*, pp. 1000–1009, 2020.
- Jianyuan Guo, Kai Han, Yunhe Wang, Han Wu, Xinghao Chen, Chunjing Xu, and Chang Xu. Distilling object detectors via decoupled features. In *CVPR*, pp. 2154–2164, 2021a.
- Xiaoyang Guo, Shaoshuai Shi, Xiaogang Wang, and Hongsheng Li. LIGA-Stereo: Learning lidar geometry aware representations for stereo-based 3D detector. In *ICCV*, pp. 3153–3163, 2021b.
- Kaiming He, Xiangyu Zhang, Shaoqing Ren, and Jian Sun. Deep residual learning for image recognition. In *CVPR*, pp. 770–778, 2016.
- Kaiming He, Haoqi Fan, Yuxin Wu, Saining Xie, and Ross Girshick. Momentum contrast for unsupervised visual representation learning. In *CVPR*, pp. 9729–9738, 2020.
- Geoffrey Hinton, Oriol Vinyals, Jeff Dean, et al. Distilling the knowledge in a neural network. In *NeurIPS Workshop*, volume 2, 2015.

- Junjie Huang and Guan Huang. BEVDet4D: Exploit temporal cues in multi-camera 3D object detection. *arXiv preprint arXiv:2203.17054*, 2022.
- Junjie Huang, Guan Huang, Zheng Zhu, and Dalong Du. BEVDet: High-performance multi-camera 3D object detection in bird-eye-view. *arXiv preprint arXiv:2112.11790*, 2021.
- Wei-Chih Hung, Henrik Kretzschmar, Vincent Casser, Jyh-Jing Hwang, and Dragomir Anguelov. LET-3D-AP: Longitudinal error tolerant 3D average precision for camera-only 3D detection. *arXiv preprint arXiv:2206.07705*, 2022.
- Yanqin Jiang, Li Zhang, Zhenwei Miao, Xiatian Zhu, Jin Gao, Weiming Hu, and Yu-Gang Jiang. PolarFormer: Multi-camera 3D object detection with polar transformers. *arXiv preprint arXiv:2206.15398*, 2022.
- Alex H Lang, Sourabh Vora, Holger Caesar, Lubing Zhou, Jiong Yang, and Oscar Beijbom. Point-Pillars: Fast encoders for object detection from point clouds. In *CVPR*, pp. 12697–12705, 2019.
- Youngwan Lee and Jongyoul Park. CenterMask: Real-time anchor-free instance segmentation. In *CVPR*, pp. 13906–13915, 2020.
- Yanwei Li, Yilun Chen, Xiaojuan Qi, Zeming Li, Jian Sun, and Jiaya Jia. Unifying voxel-based representation with transformer for 3D object detection. In *NeurIPS*, 2022a.
- Yinhao Li, Zheng Ge, Guanyi Yu, Jinrong Yang, Zengran Wang, Yukang Shi, Jianjian Sun, and Zeming Li. BEVDepth: Acquisition of reliable depth for multi-view 3D object detection. *arXiv preprint arXiv:2206.10092*, 2022b.
- Zhiqi Li, Wenhui Wang, Hongyang Li, Enze Xie, Chonghao Sima, Tong Lu, Qiao Yu, and Jifeng Dai. BEVFormer: Learning bird’s-eye-view representation from multi-camera images via spatiotemporal transformers. In *ECCV*, pp. 1–18, 2022c.
- Yingfei Liu, Tiancai Wang, Xiangyu Zhang, and Jian Sun. PETR: Position embedding transformation for multi-view 3D object detection. In *ECCV*, pp. 531–548, 2022a.
- Yingfei Liu, Junjie Yan, Fan Jia, Shuailin Li, Qi Gao, Tiancai Wang, Xiangyu Zhang, and Jian Sun. PETRv2: A unified framework for 3D perception from multi-camera images. *arXiv preprint arXiv:2206.01256*, 2022b.
- Zhijian Liu, Haotian Tang, Alexander Amini, Xinyu Yang, Huizi Mao, Daniela Rus, and Song Han. BEVFusion: Multi-task multi-sensor fusion with unified bird’s-eye view representation. *arXiv preprint arXiv:2205.13542*, 2022c.
- Zhuang Liu, Hanzi Mao, Chao-Yuan Wu, Christoph Feichtenhofer, Trevor Darrell, and Saining Xie. A ConvNet for the 2020s. In *CVPR*, pp. 11976–11986, 2022d.
- Jiachen Lu, Zheyuan Zhou, Xiatian Zhu, Hang Xu, and Li Zhang. Learning ego 3D representation as ray tracing. In *ECCV*, pp. 129–144, 2022.
- Liang Peng, Fei Liu, Zhengxu Yu, Senbo Yan, Dan Deng, Zheng Yang, Haifeng Liu, and Deng Cai. LiDAR point cloud guided monocular 3D object detection. In *ECCV*, pp. 123–139, 2022.
- Jonah Philion and Sanja Fidler. Lift, splat, shoot: Encoding images from arbitrary camera rigs by implicitly unprojecting to 3D. In *ECCV*, pp. 194–210, 2020.
- Adriana Romero, Nicolas Ballas, Samira Ebrahimi Kahou, Antoine Chassang, Carlo Gatta, and Yoshua Bengio. FitNets: Hints for thin deep nets. In *ICLR*, 2014.
- Martijn J Schuemie, Peter Van Der Straaten, Merel Krijn, and Charles APG Van Der Mast. Research on presence in virtual reality: A survey. *CyberPsychology & Behavior*, 4(2):183–201, 2001.
- Shaoshuai Shi, Chaoxu Guo, Li Jiang, Zhe Wang, Jianping Shi, Xiaogang Wang, and Hongsheng Li. PV-RCNN: Point-voxel feature set abstraction for 3D object detection. In *CVPR*, pp. 10529–10538, 2020.

- Pei Sun, Henrik Kretzschmar, Xerxes Dotiwalla, Aurelien Chouard, Vijaysai Patnaik, Paul Tsui, James Guo, Yin Zhou, Yuning Chai, Benjamin Caine, et al. Scalability in perception for autonomous driving: Waymo open dataset. In *CVPR*, pp. 2446–2454, 2020.
- Yonglong Tian, Dilip Krishnan, and Phillip Isola. Contrastive representation distillation. In *ICLR*, 2019a.
- Zhi Tian, Chunhua Shen, Hao Chen, and Tong He. FCOS: Fully convolutional one-stage object detection. In *ICCV*, pp. 9627–9636, 2019b.
- Tai Wang, Xinge Zhu, Jiangmiao Pang, and Dahua Lin. FCOS3D: Fully convolutional one-stage monocular 3D object detection. In *ICCV Workshop*, pp. 913–922, 2021a.
- Tai Wang, Qing Lian, Chenming Zhu, Xinge Zhu, and Wenwei Zhang. MV-FCOS3D++: Multi-view camera-only 4D object detection with pretrained monocular backbones. *arXiv preprint arXiv:2207.12716*, 2022a.
- Tai Wang, ZHU Xinge, Jiangmiao Pang, and Dahua Lin. Probabilistic and geometric depth: Detecting objects in perspective. In *CoRL*, pp. 1475–1485. PMLR, 2022b.
- Tao Wang, Li Yuan, Xiaopeng Zhang, and Jiashi Feng. Distilling object detectors with fine-grained feature imitation. In *CVPR*, pp. 4933–4942, 2019a.
- Yan Wang, Wei-Lun Chao, Divyansh Garg, Bharath Hariharan, Mark Campbell, and Kilian Q Weinberger. Pseudo-lidar from visual depth estimation: Bridging the gap in 3D object detection for autonomous driving. In *CVPR*, pp. 8445–8453, 2019b.
- Yingjie Wang, Qiuyu Mao, Hanqi Zhu, Yu Zhang, Jianmin Ji, and Yanyong Zhang. Multi-modal 3D object detection in autonomous driving: a survey. *arXiv preprint arXiv:2106.12735*, 2021b.
- Yue Wang and Justin M Solomon. Object dgcn: 3D object detection using dynamic graphs. In *NeurIPS*, volume 34, pp. 20745–20758, 2021.
- Yue Wang, Vitor Campagnolo Guizilini, Tianyuan Zhang, Yilun Wang, Hang Zhao, and Justin Solomon. DETR3D: 3D object detection from multi-view images via 3D-to-2D queries. In *CoRL*, pp. 180–191, 2022c.
- Enze Xie, Zhiding Yu, Daquan Zhou, Jonah Philion, Anima Anandkumar, Sanja Fidler, Ping Luo, and Jose M Alvarez. M2BEV: Multi-camera joint 3D detection and segmentation with unified birds-eye view representation. *arXiv preprint arXiv:2204.05088*, 2022.
- Yan Yan, Yuxing Mao, and Bo Li. SECOND: Sparsely embedded convolutional detection. *Sensors*, 18(10):3337, 2018.
- Chenhongyi Yang, Mateusz Ochal, Amos Storkey, and Elliot J Crowley. Prediction-guided distillation for dense object detection. In *ECCV*, pp. 123–138, 2022a.
- Zhendong Yang, Zhe Li, Xiaohu Jiang, Yuan Gong, Zehuan Yuan, Danpei Zhao, and Chun Yuan. Focal and global knowledge distillation for detectors. In *CVPR*, pp. 4643–4652, 2022b.
- Zhendong Yang, Zhe Li, Mingqi Shao, Dachuan Shi, Zehuan Yuan, and Chun Yuan. Masked generative distillation. In *ECCV*, pp. 53–69, 2022c.
- Tianwei Yin, Xingyi Zhou, and Philipp Krahenbuhl. Center-based 3d object detection and tracking. In *CVPR*, pp. 11784–11793, 2021.
- Linfeng Zhang and Kaisheng Ma. Improve object detection with feature-based knowledge distillation: Towards accurate and efficient detectors. In *ICLR*, 2020.
- Yunpeng Zhang, Jiwen Lu, and Jie Zhou. Objects are different: Flexible monocular 3D object detection. In *CVPR*, pp. 3289–3298, 2021.
- Yunpeng Zhang, Zheng Zhu, Wenzhao Zheng, Junjie Huang, Guan Huang, Jie Zhou, and Jiwen Lu. BEVerse: Unified perception and prediction in birds-eye-view for vision-centric autonomous driving. *arXiv preprint arXiv:2205.09743*, 2022.

Zhaohui Zheng, Rongguang Ye, Ping Wang, Dongwei Ren, Wangmeng Zuo, Qibin Hou, and Ming-Ming Cheng. Localization distillation for dense object detection. In *CVPR*, pp. 9407–9416, 2022.

Xingyi Zhou, Dequan Wang, and Philipp Krähenbühl. Objects as points. *arXiv preprint arXiv:1904.07850*, 2019.

A IMPLEMENTATION OF CRITIC g

Firstly, we adopt bilinear $F_{bilinear}$ to obtain the paired 2D/3D features f_i^{2D}, f_i^{3D} on student and teacher BEV features maps F^{2D}, F^{3D} according to the reference location r_i predicted by each student query q_i :

$$f_i^{2D} = F_{bilinear}(F^{2D}, r_i), \quad f_i^{3D} = F_{bilinear}(F^{3D}, r_i). \quad (14)$$

Note that we adopt query points from 6 stages which actually form 900×6 feature pairs. Each 2D and 3D feature located at the same position are viewed as a positive pair. We use separate projection heads for 2D and 3D features since they originated from different modalities. Each projection head is a 3-layer MLP (g^{2D}, g^{3D}) and the final loss can be written as

$$\begin{aligned} x_i^{2D} &= g^{2D}(f_i^{2D}), \quad x_i^{3D} = g^{3D}(f_i^{3D}) \\ L &= -\log \frac{\exp(x_i^{2D} \cdot x_i^{3D} / \tau)}{\sum_{j=0, j \neq i}^K \exp(f_i^{2D} \cdot f_j^{3D} / \tau)} \end{aligned} \quad (15)$$

where τ is the temperature. Different from the original implementation in (He et al., 2020), we do not collate samples from other cards during distributed training since there are enough negative samples (5400-1=5399) for each card.

B MORE EXPERIMENTAL RESULTS

B.1 EXPERIMENTS ON BEVFORMER WITH LARGER BACKBONES

Instead of the results conducted on ResNet-50 backbone, we also provide detailed experiments with stronger backbones, ResNet-101. We keep all experimental settings the same in Section 4.5 except for the image backbone and the results are shown in Table 8. From the table, we can conclude that BEVDistill can still consistently improve the competitive baseline BEVFormer, even with a much stronger ResNet-101 backbone by more than 2.3 and 1.8 NDS.

Table 8: Experimental results of BEVDistill with BEVFormer on ResNet-101 DCN backbone, under both single-frame and multi-frame settings.

Detector	Setting	NDS↑	mAP↑
BEVFormer	Teacher	67.4	61.5
	Student	44.5	37.4
	+BEVDistill	46.8(+2.3)	38.9(+1.5)
BEVFormer-T	Teacher	67.4	61.5
	Student	50.6	40.5
	+BEVDistill	52.4(+1.8)	41.7(+1.2)

B.2 DISTILLING TO A LIGHTWEIGHT BACKBONE

Knowledge distillation is actually one of the most common solutions to model compression. It is usually adopted to transfer useful information from a large stronger model to a lightweight weaker model, which is suitable for deployment on the edge. Considering that vision-based detectors are fed with a batch of images for surrounding view inputs, it is extremely important to reduce the size of the image backbone. With this in mind, we conduct experiments with smaller backbones, including ResNet-18 and MobileNetV2, which is a more demanded setting in real applications. The final results are shown in Table 9. BEVDistill improves the ResNet-18 and MobileNetV2 backbones by more than 2.1/1.7 NDS, pointing its great potential for resource-limited applications including autonomous driving and edge computing.

Table 9: Experimental results of BEVDistill on smaller image backbones: ResNet-18 and MobileNetV2 on nuScenes validation subset.

Detector	Backbone	Setting	NDS↑	mAP↑
BEVFormer	ResNet-18	Teacher	67.4	61.5
		Student	37.3	30.0
		+ BEVDistill	40.2(+2.9)	32.0(+2.0)
BEVFormer-T	ResNet-18	Teacher	67.4	61.5
		Student	43.7	32.1
		+ BEVDistill	45.8(+2.1)	33.9(+1.8)
BEVFormer	MobileNet-V2	Teacher	67.4	61.5
		Student	37.0	29.3
		+ BEVDistill	38.8(+1.8)	30.8(+1.5)
BEVFormer-T	MobileNet-V2	Teacher	67.4	61.5
		Student	43.1	32.0
		+ BEVDistill	44.8(+1.7)	33.5(+1.5)

Table 10: Experimental results of BEVDepth with BEVDepth on ResNet-50 backbone.

Detector	Setting	NDS↑	mAP↑
BEVDepth	Teacher	66.4	60.3
	Student	44.0	31.7
	+BEVDistill	45.2(+1.2)	33.0(+1.3)

B.3 EXPERIMENTS ON BEVDEPTH

To fully exploit the capability of this simple framework, we extend it to adapt the current state-of-the-art multi-view 3D detector, BEVDepth. Since BEVDepth and BEVFormer both share BEV space as the intermediate feature representation, we can directly apply dense feature distillation. As for the instance distillation, BEVDepth conducts dense prediction similar to CenterPoint. Therefore, we directly choose CenterPoint as our teacher model and only conduct instance distillation on the foreground regions (*i.e.*, the center of ground truth objects). We conduct experiments on ResNet-50 backbone on nuScenes 1/2 training subset and report the results on validation subset in Table 10. Surprisingly, BEVDistill can still improve its vanilla baseline by 1.2 NDS, even though BEVDepth has already leveraged the information from LiDAR data with explicit depth supervision.

Table 11: Experimental results of BEVDistill with MV-FCOS3D++ and MV-FCOS4D++ on Waymo Open Dataset. Following the practice in (Wang et al., 2022a), we sample every 5 frame to form the training set.

Detector	Backbone	BEVDistill	mAPL↑	mAP↑	mAPH↑
MV-FCOS3D++	ResNet-50	✓	32.6	45.1	42.7
	ResNet-50		34.3	46.8	44.4
MV-FCOS4D++	ResNet-50	✓	34.0	46.5	43.8
	ResNet-50		35.1	47.5	44.9

B.4 EXPERIMENTS ON WAYMO OPEN DATASET

In this section, we report BEVDistill on another competitive public dataset, Waymo Open Dataset (Sun et al., 2020) to further demonstrate the generalization of our approach. Due to the characteristics of the camera-based detections, instead of adopting original mAP metrics, we choose the official

released LET-mAP (Hung et al., 2022) to evaluate the model performance. Since most multi-view 3D detectors do not report their performances on Waymo dataset, we select another competitive multi-view 3D detector, MV-FCOS3D++ (Wang et al., 2022a), which achieves 2rd place at the Waymo Open Dataset Challenge–Camera-Only Track, as our baseline. The follow the same experimental settings in the official MV-FCOS3D++ repository. We select our teacher model as SEC-OND to adapt with the Anchor3DHead used by MV-FCOS3D++. The final results are reported in Table 11. It can be concluded that BEVDistill can consistently improves MV-FCOS3D++ and MV-FCOS4D++ (multi-frames input version of MV-FCOS3D++) by 1.7/1.1 mAPL, respectively, indicating the robustness and general of the proposed method.

C DISCUSSIONS

C.1 WHY KL DIVERGENCE DISTILLATION ON SPARSE QUERY LOGITS FAILS TO IMPROVE?

KL logit distillation has been proven to be effective in plenty of works (Tian et al., 2019a; Hinton et al., 2015). However, it fails to yield improvements under the cross-modal distillation. By visualizing the training data and the predicted logits, we attribute one reason to this problem: for most previous distillations, both teacher and student are fed with the data in the same modality. Therefore, both of them should behave in a similar manner in every region. Such a hypothesis may not hold under different modalities: due to the characteristics of the modal sensor, the information collected by each sensor can be diverse. For instance, even if one person is occluded by another one in the image view, he may still be perceived by the LiDAR sensors. Besides, some instances can be easily detected by one modal sensor, while it may be hard on the other one, leading to different logits distribution predicted by the model. Directly forcing the student to mimic such distribution can deteriorate the inner knowledge learned by the student itself. Different from logit imitation, the contrastive paradigm only enforces the contexts encoded in each modality are the same, providing the freedom for the model to learn the representation encoded in the respective modality.

C.2 WHAT DOES THE MODEL LEARN FROM ITS CROSS-MODAL TEACHER?

Different from the previous knowledge distillation framework, BEVDistill leverages LiDAR models to transfer knowledge. A natural question is: what does a multi-view vision-based student learn from its LiDAR-based 3D teacher? Actually, it is hard to figure out the explicit knowledge learned by the student, however, we can get some hints to some extent by comparing the detection performance evaluated from various aspects. The detailed results are shown in Table 12.

Table 12: Detailed metrics comparison between BEVFormer and BEVDistill on nuScenes validation dataset with ResNet-50 image backbone.

Method	NDS	mAP	mATE	mASE	mAOE	mAVE	mAAE
BEVFormer	42.3	35.2	0.755	0.271	0.428	0.870	0.208
+ BEVDistill	45.7	38.6	0.693	0.264	0.399	0.802	0.199
BEVFormer-T	48.8	38.3	0.707	0.281	0.435	0.414	0.194
+ BEVDistill	51.5	40.7	0.663	0.268	0.393	0.374	0.184

From the table we can find that the most significant improvements are mainly related to object localization, orientation and velocity estimation. LiDAR point clouds provide accurate localization information, which is of great benefit to localizing the object, including the absolute 3D space and its orientation. Both of them are more challenging to acquire from the camera view only. Note that the velocity estimation gets a 10% enhancement since the LiDAR model introduces more spatial information (*i.e.*, the LiDAR model takes 10 consecutive sweeps of point clouds as inputs instead of a single frame). As for the attribute prediction, which is mostly bound up with the classification tasks, BEVDistill fails to gain satisfying performance. We attribute the reason to the deficiency of point clouds in semantic representation compared to the imagery data, which may also account for the failure in KL distillation on the classification branch discussed in Section 3.2.2.

D QUALITATIVE RESULTS

We provide some qualitative results in Figure 2. More visualizations can refer to the supplementary materials, which are presented in a video format.

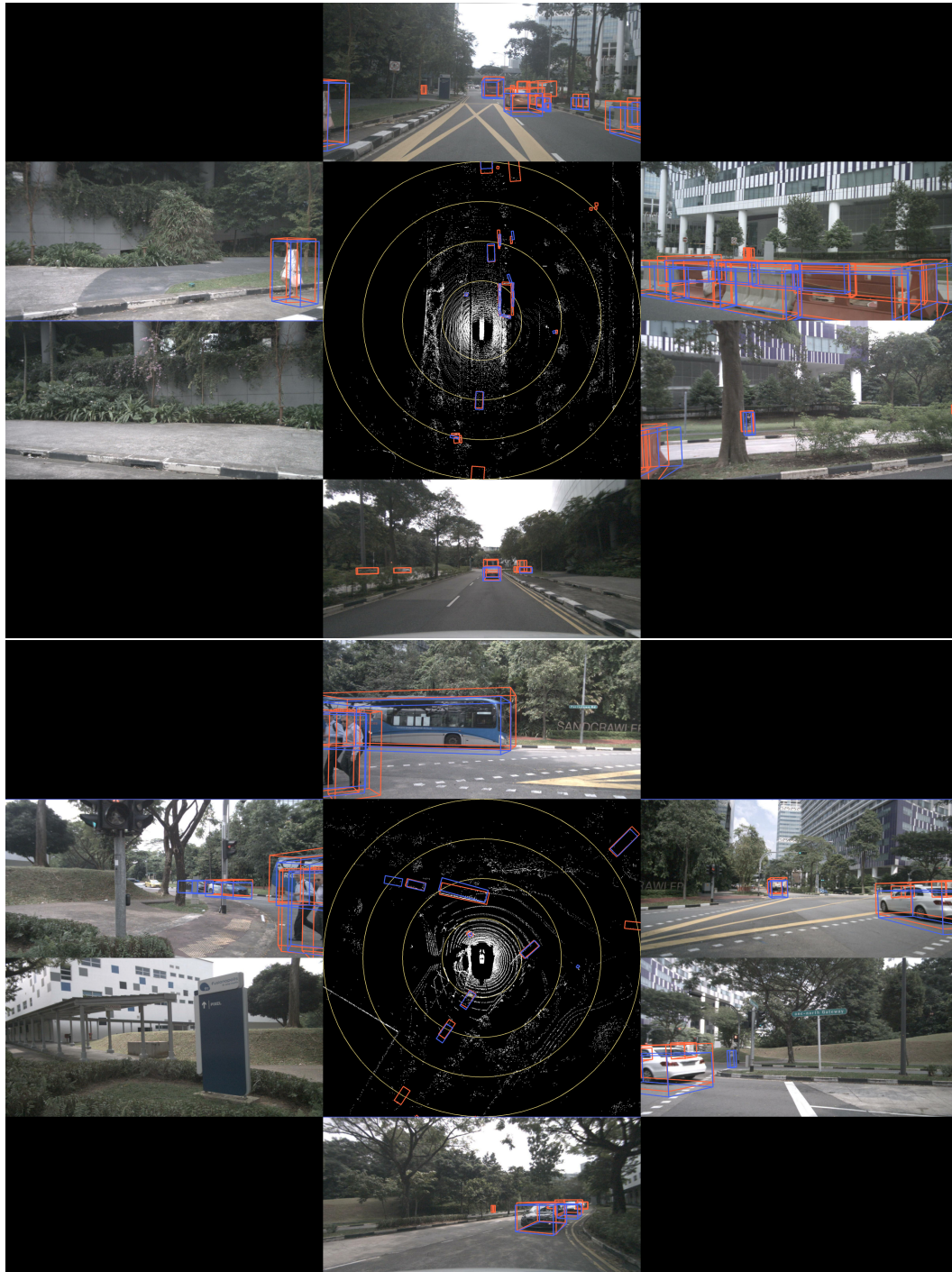


Figure 2: Visualization of the detection results predicted by BEVDistill. Best view in color: the prediction and ground truth are in blue and orange, respectively.